NJC

Accepted Manuscript

This is an *Accepted Manuscript*, which has been through the Royal Society of Chemistry peer review process and has been accepted for publication.

Accepted Manuscripts are published online shortly after acceptance, before technical editing, formatting and proof reading. Using this free service, authors can make their results available to the community, in citable form, before we publish the edited article. We will replace this *Accepted Manuscript* with the edited and formatted *Advance Article* as soon as it is available.

You can find more information about *Accepted Manuscripts* in the Information for Authors.

Please note that technical editing may introduce minor changes to the text and/or graphics, which may alter content. The journal's standard Terms & Conditions and the Ethical guidelines still apply. In no event shall the Royal Society of Chemistry be held responsible for any errors or omissions in this *Accepted Manuscript* or any consequences arising from the use of any information it contains.

ROYAL SOCIETY OF CHEMISTRY

www.rsc.org/njc

Efficient visible light photocatalytic activity and enhanced stability over $BiOBr/Cd(OH)_2$ Heterostructures

Bilal Masood Pirzada[a], Owais Mehraj[a], Niyaz A. Mir[b], Mohammad Zain Khan[a], Suhail Sabir[a]*

[a]*Department of Chemistry, Aligarh Muslim University, Aligarh – 202002, India*

[b]*Solid State & Structural Chemistry Unit, Indian Institute of Science Bangalore-560012, India*

*Corresponding author: Suhail Sabir: *drsuhailsabir@gmail.com*

Correspondence:

Dr Suhail Sabir, Department of Chemistry, Aligarh Muslim University, Aligarh, India, 202002.

Email: *drsuhailsabir@gmail.com*

Phone: +91-571-2700920-ext-3366

Abstract:

Novel BiOBr/$Cd(OH)_2$ heterostructures were synthesized by a facile chemical bath method under ambient conditions. A series of BiOBr/$Cd(OH)_2$ heterostructures were obtained by tuning the Bi/Cd molar ratios. The obtained heterostructures were characterized by the Powder X-ray Diffraction (PXRD), Scanning Electron Microscopy (SEM), Transmission Electron Microscopy (TEM) and Energy Dispersive Spectroscopy (EDS). Optical properties were studied by UV-Visible spectroscopy, Diffuse Reflectance Spectroscopy and Photoluminescence (PL). Photocatalytic studies on Rhodamine B (RhB) under visible light irradiation showed that the heterostructures are very efficient photocatalysts in mild basic medium. Scavenger test studies confirmed that the photogenerated holes and superoxide radicals ($O_2^{\bullet-}$) are the main active species responsible for RhB degradation. Comparison of Photoluminescence (PL) intensity suggested that an inhibited charge recombination is crucial for the degradation process over these photocatalysts. Moreover, relative positioning of the valence and conduction band edges of the semiconductors, $O_2/O_2^{\bullet-}$, $^{\bullet}OH/H_2O$ redox potential and HOMO−LUMO levels of RhB appears to be responsible for the hole-specificity of degradation. Photocatalytic recycling experiments indicated high stability of the catalysts in the reaction medium without any significant loss of activity. The study hence concludes that the heterojunction constructed between the $Cd(OH)_2$ and BiOBr interfaces play a crucial role in influencing the charge carrier dynamics and their photocatalytic activity.

Keywords: Cadmium Hydroxide, Bismuth oxybromide, Heterostructure, Charge transfer, Photocatalysis

1. Introduction

Heterogeneous photocatalysis has evolved as a viable technology for the control of environmental pollution related issues and energy conversion[1]. Till date various kinds of catalyst semiconductor materials, including metal oxides[2], sulphides[3], nitrides[4], and their mixed solid solutions[5, 6] have been tried as photocatalysts responsive to both the UV and visible light wavelengths. Primarily, TiO_2 received wide attention due to its excellent photocatalytic activity, chemical stability, and non-toxicity[7]. However, it has limited practical application due to large band gap ~3.2eV and rapid recombination of photogenerated charge carriers[8].

In order to overcome the limitation and effectively control the photocorrosion, the various attempts include encapsulation of electron acceptors on functionalized semiconductors, immobilization of semiconductor photocatalyst in redox functionalized polymers and electrostatic association of electron acceptors at the semiconductor surface. Transition metal ion doping is one approach for acquiring a visible response by introducing intermediate impurity energy levels.[9, 10]The efficiency of photocatalyst is considerably enhanced by coupling with a foreign metal oxide. [11, 12a] Currently, coupling of semiconductors with graphene is widely recognized to be a viable strategy to improve the photocatalytic performance for, an electronically conductive 2D platform enabling the acceptance and shuttle of photogenerated electrons from band-gap-excitation of semiconductors.[12b,c,d] Recent studies have also revealed that some physical and chemical properties of TiO_2, such as light absorption, photocatalytic reactivity and selectivity etc., can be modulated by its defect disorder.[12e]

Heterostructure construction between two different semiconductors has also been extensively applied in many fields including photocatalysis and solar energy conversion[13, 14], because heterojunctions control behaviour of photogenerated charges, such as the direction of

transportation, the distance for separation, and the recombination rate. [15, 16] Furthermore, the internal electric field built at a heterojunction interface can greatly decrease the charge-carrier recombination and increase their lifetimes, thus enhancing the photocatalytic activity.[17]

As a group of V–VI–VII semiconductors, bismuth oxyhalides are of immense importance due to their optical properties and promising industrial applications, such as in photocatalysis, ferroelectric materials, pigments etc.[18, 19]In particular, BiOBr has received wider interest because of its good visible light photocatalytic activity. Previous research reported BiOBr nanostructures with various architectures, such as nanoparticles[20], nanoplates[21], 3D hierarchical structures, including flowerlike microspheres and hollow flower-like microspheres.[22, 23]All were found to exhibit good catalytic activity. It crystallizes in the tetragonal matlockite (PbFCl) structure, which comprises of a layer of $[Bi_2O_2]$ slabs interleaved by double slabs of halogen atoms.[24] These layered structures with partially distorted polyhedrons are beneficial to the charge transfer and photocatalytic properties.[25]

However, it is important to further improve the photo-catalytic activity of the pure BiOBr for practical applications. One strategy is to decorate the host BiOBr with noble metals, which can increase the rate of transfer of the photo-induced charge carriers and enhance the photocatalytic activity.[26] Another attractive strategy is through the combination of BiOBr with other semiconductor moieties to form heterojunctions such as, C_3N_4[27], AgBr[28], Bi_2WO_6[29] etc., to facilitate the separation of the electrons and holes and to improve photocatalytic activity.

In the present study, novel BiOBr/$Cd(OH)_2$ heterostructures with efficient photocatalytic activities have been synthesized. Cadmium hydroxide ($Cd(OH)_2$) is a wide band gap (~3.2-3.5 eV) semiconductor material and is not responsive to visible light.[30] Hence, our efforts were directed to sensitize the activity in $Cd(OH)_2$ under visible light. The energy levels of BiOBr and $Cd(OH)_2$ materials are well-matched with a sign of overlapping, and therefore

their combination to prepare $BiOBr/Cd(OH)_2$ heterostructures is thought to be a suitable method to separate the photogenerated charges. The presence of Bi shifts the absorption band edge in the visible region due to the formation of a hybridized valence band comprising of Bi 6s and O 2p states[31] and facilitates oxidation reaction because of high mobility of photo-generated holes.[32-34]

To the best of our knowledge, there is no report on the fabrication of coupled $BiOBr/Cd(OH)_2$ heterostructures and their photocatalytic performances. Herein, we report a low-temperature method to synthesize $BiOBr/Cd(OH)_2$ heterostructures in one step. By simply tuning the Bi/Cd molar ratios, the morphology and the subsequent photochemical properties of the heterostructures were controlled. The photocatalysts synthesized were studied for the degradation of potentially toxic and carcinogenic RhB dye under visible light irradiation.[34]

On the basis of experimental and theoretical results, a possible mechanism for the photocatalytic degradation by the $BiOBr/Cd(OH)_2$ composites was proposed and corroborated by radical scavenger experiments and photoluminescence spectroscopy.

2. Experimental

2.1. Synthesis of Photocatalyst

All the reagents for synthesis and analysis were of analytical grade, procured from Sigma Aldrich and Merck India, and were used without further treatment or modification. $BiOBr/Cd(OH)_2$ heterostructures were synthesized by a facile chemical bath method at ambient temperature.[17] Typically, $Cd(NO_3)_2.4H_2O$ was added to 40 mL of deionized water containing a stoichiometric amount of NaOH (Cd/OH molar ratio of 1:2) with constant stirring resulting in a white precipitate. Then, a stoichiometric amount of NaBr was added, and the mixture was stirred for 30 min. at room temperature. Subsequently, different stoichiometric amounts of $Bi(NO_3)_3.5H_2O$ were added to the resultant mixed solution. The

Bi/Cd molar percentages were kept to 0, 30, 50, 70 (denoted as CDH, BC-30, BC-50, and BC-70), respectively. After being stirred for another 30 min at room temperature, the resulting mixtures were heated at 80^{o}C for 2h on a water bath.

Finally, the precipitates were collected, washed thoroughly with deionised water and ethanol, and dried at 50 ^{o}C in air. For comparison, pure BiOBr was prepared by the same procedure without the addition of $Cd(NO_3)_2$.$4H_2O$ and NaOH.

2.2. Characterization

The crystal structure of the composites were analysed by powder X-ray diffraction (PXRD, Miniflex-TM II Benchtop, Rigaku Cooperation, Tokyo, Japan). The surface morphology of the composites was characterized by Scanning Electron Microscopy (JEOL, JSM6510LV) and the heterojunction formation was analyzed by High Resolution Transmission Electron Microscopy (JEOL, JEM2100F) and Selected Area Electron Diffraction (SAED). The UV–Vis absorption spectra were obtained in the range of 190–700nm by UV-Vis Spectrophotometer (Shimadzu UV-1601). UV–Vis Diffuse Reflectance Spectra (UV-DRS) were obtained using a Puxi, UV1901 spectrometer with $BaSO_4$ as a reference, and the chemical compositions of the catalysts were examined by energy dispersive X-ray spectroscopy (EDS, JEOL, JSM6510LV). To study the recombination of photo induced charge carriers, photo-luminescence spectra (PL, Hitachi F-7000, 280 nm) were measured. Cadmium ion leaching by the catalyst was analyzed by Atomic Absorption Spectroscopy (GBC-932 Plus flame atomic absorption spectrometer, Australia).

2.3. Evaluation of Photocatalytic Activity

The photocatalytic activity of the nanocomposites was assessed by monitoring decolorization of Rhodamine B in presence of visible light. The photocatalytic experiments were carried in an immersion well photoreactor (consisting of inner and outer jacket) made up of Pyrex glass, equipped with a magnetic bar, water circulating jacket and a passage for molecular oxygen. A

detailed description of photoreactor is given elsewhere.[35] Irradiations were carried out using a visible light halogen linear lamp (500 W, 9500 Lumens). The reaction temperature was kept constant at 20±0.3°C using refrigerated circulating liquid bath. Before irradiation experiments, 300 mL of the dye solution of appropriate concentration containing the desired quantity of the catalyst (1 gL^{-1}) and a predetermined amount of 2mM NaOH solution, was magnetically stirred, while the solution was continuously purged with atmospheric oxygen for at least 20 min in the dark to attain adsorption–desorption equilibrium between the dye solution and the catalyst surface. Afterwards, first sample (0 min) was taken out and the irradiation was started. During irradiation, samples of 5 mL were withdrawn at constant time intervals, centrifuged and the supernatant was subsequently analyzed. The change in absorbance of the dye aliquots was followed at its λ_{max} (554nm) as a function of irradiation time. The observed absorbance spectra are in accordance with Beer-Lambert Law in the range of examined dye concentration. The concentration of dye was calculated by standard calibration curve obtained from the absorbance of the dye at different known concentrations. The photocatalytic experiments were repeated three times in order to check the reproducibility of the experimental results. The accuracy of the optical density was found to be within ±5%.[35]

The consistency in activity of the catalyst was analyzed by the recycling experiments. After the first attempt of the photocatalysis experiment, the catalyst was retrieved from the photoreactor and the aliquots by centrifugation. The retrieved catalyst was thoroughly washed by deionised water and distilled ethanol. The catalyst was dried at 40°C for 12 hr and then reused in the next cycle of the photocatalysis experiment. Same way, the experiment was repeated for a set of cycles to monitor the loss in efficiency of the catalyst after repetitive use. The photocatalyst concentration was optimized by a series of photocatalysis experiments. Higher concentrations of photocatalyst were thought to absorb more incident photons and

produce more photogenerated charges carriers, but past a particular concentration, the particles suspended in the solution cause shielding and light scattering, affecting the light transmittance in solution. Moreover, the decreasing transmittance may enhance recombination as the photons could not be continuously injected onto the photocatalyst particles.[36] Similarly the initial dye solution concentration has significant influence on the activity as it affects the light penetration into solution. This result was consistent with literature for the effect of initial concentration on photocatalysis.[37]

The degradation efficiency (%) was calculated as follows:

$$Degradation\ Efficiency\ (\%) = \frac{C_o - C}{C_o} \times 100 \qquad (1)$$

where C_0 is the initial concentration of RhB, and C is the time-dependent concentration of dye upon irradiation. According to a simplified Langmuir–Hinshelwood (L–H) kinetic model, the following first order kinetic equation can be used to describe photocatalytic RhB degradation.[38]

$$\ln\left(\frac{C_o}{C_t}\right) = k_{app}t \qquad (2)$$

Where C_0 and C are the concentrations of dye in solution at times 0 and t respectively, and k_{app} is the apparent first-order rate constant (min^{-1}).

To determine the effect of resultant reactive oxygen species (ROS), various quencher species were added to the reaction system in the manner similar to the photocatalytic experiment. The dosage of quenchers was referred to the previous studies.[39-41]

3. Results and Discussion

3.1. Crystallographic Study

The powder XRD spectra for the as-prepared BiOBr/$Cd(OH)_2$ nanocomposites are shown in Fig. 1.

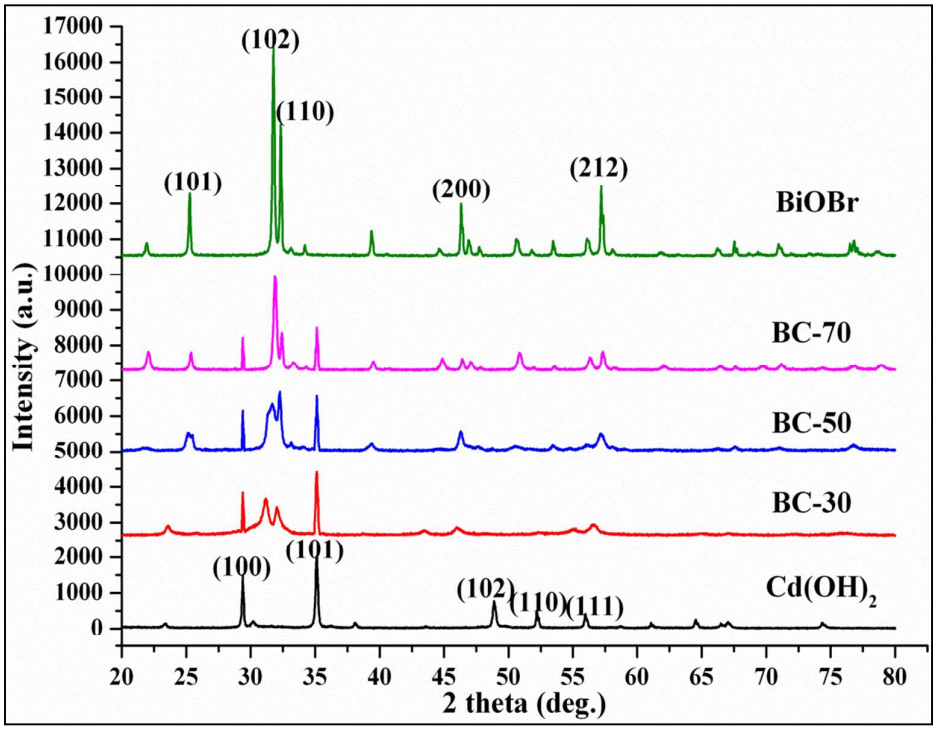

Fig.1. XRD pattern of the different samples

Characteristic diffraction peaks for $Cd(OH)_2$ were detected at 2Θ angles of 29.38°, 35.12°, 48.9°, 52.2°, and 55.98° and were attributed to the (1 0 0), (1 0 1), (1 0 2), (1 1 0) and (1 1 1) crystal planes of the hexagonal $Cd(OH)_2$ crystal, respectively.[42] The characteristic diffraction peaks for BiOBr were detected at 2θ angles of 25.2°, 31.7°, 32.2°, 46.2°and 57.1°, and were attributed to the (1 0 1), (1 0 2), (1 1 0), (2 0 0), and (2 1 2) crystal planes, of the BiOBr crystal, respectively.[43a] The composites prepared are considered to possess a highly crystalline nature as the diffraction peaks are relatively acute. In the diffraction patterns of the

$BiOBr/Cd(OH)_2$ composites, both $Cd(OH)_2$ and BiOBr were detected, indicating that the synthesized composite materials possess both the constituent phases. However, when the BiOBr content increased from 30 mole% to 70 mole%, the intensity of the BiOBr peaks increased, whereas the $Cd(OH)_2$ peak intensities decreased, which may be caused by the gradual covering of the $Cd(OH)_2$ surface by the BiOBr.

3.2. Microscopic Analysis

The surface morphology of the $BiOBr/Cd(OH)_2$ composite samples was studied by SEM (Fig. 2).

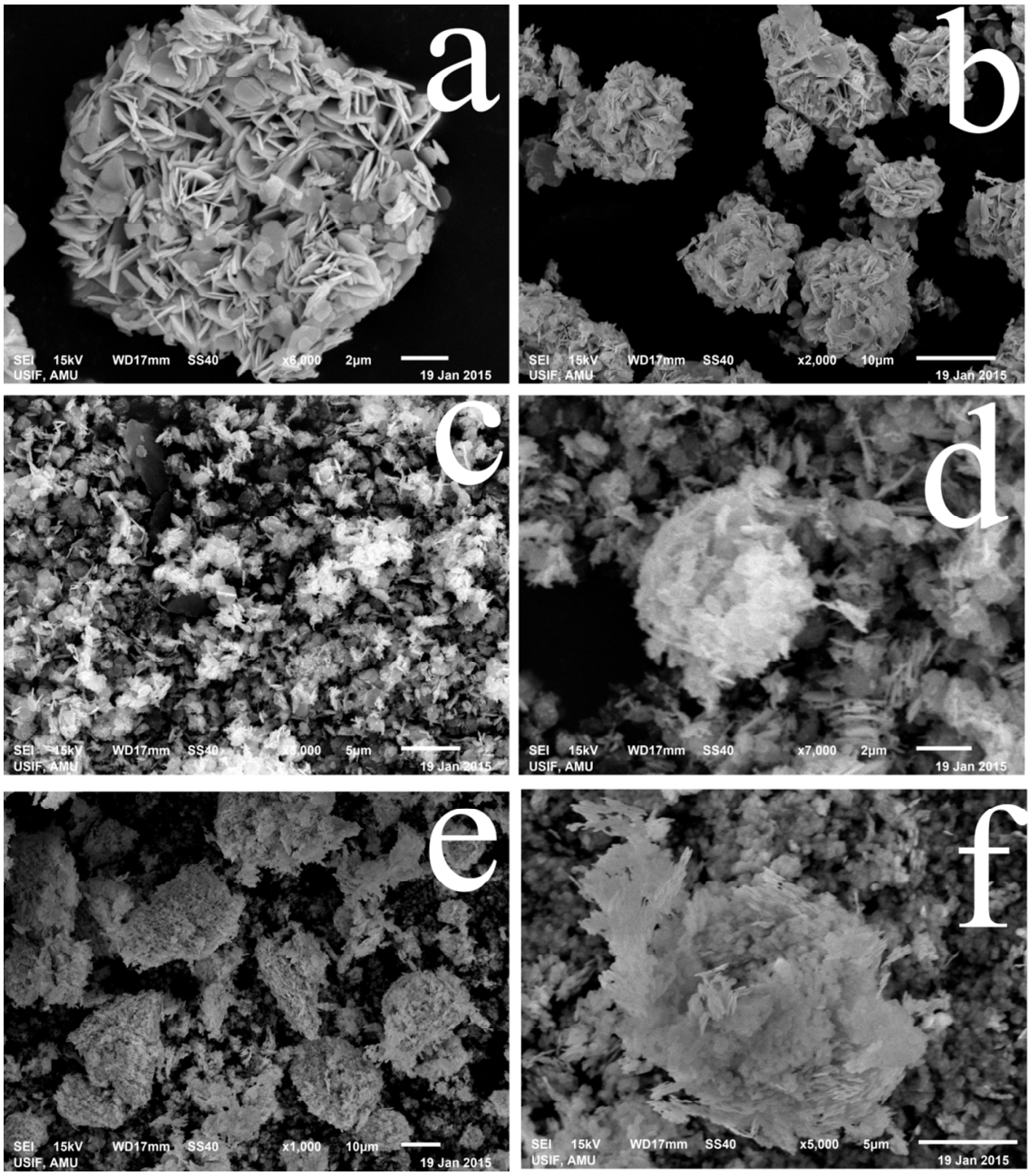

Fig.2. SEM images: (a-b) flower like cluster of BiOBr, (c-d) $Cd(OH)_2$ nanoparticles, (e-f) BC-50 nanocomposite

As shown in Fig. 2(a-b), three dimensional (3D) BiOBr hierarchical microspheres (with diameters of 10-15 μm) constructed by numerous petal like interlaced nanosheets were observed. The nanosheets are aligned from the sphere centre to the surface, and give a floral appearance. The microstructure of the $Cd(OH)_2$ nanoparticles is shown in Fig. 2(c-d). Agglomerates were observed, with sizes varying from 200 to 250 nm, due to small size and

large surface energy. Fig. 2(e-f) shows the SEM image of BC-50 sample. The $Cd(OH)_2$ nanoparticles were observed to be in intimate proximity to the surface of BiOBr, resulting in effective coupling, which was thought to facilitate the charge transfer. In addition, the $Cd(OH)_2$ adhered to the BiOBr surface possessed much smaller grain sizes than the pure $Cd(OH)_2$ nanoparticles as the BiOBr microspheres suppressed agglomeration of the $Cd(OH)_2$ nanoparticles.

The HRTEM images in Fig. 3 show nanosheets of BiOBr (Fig. 3(a)) and $Cd(OH)_2$ nanorods (Fig 3(b)). Fig. 3(c-d) exhibits the HRTEM images of the heterostructured BiOBr/ $Cd(OH)_2$ nanocomposite (BC-50).

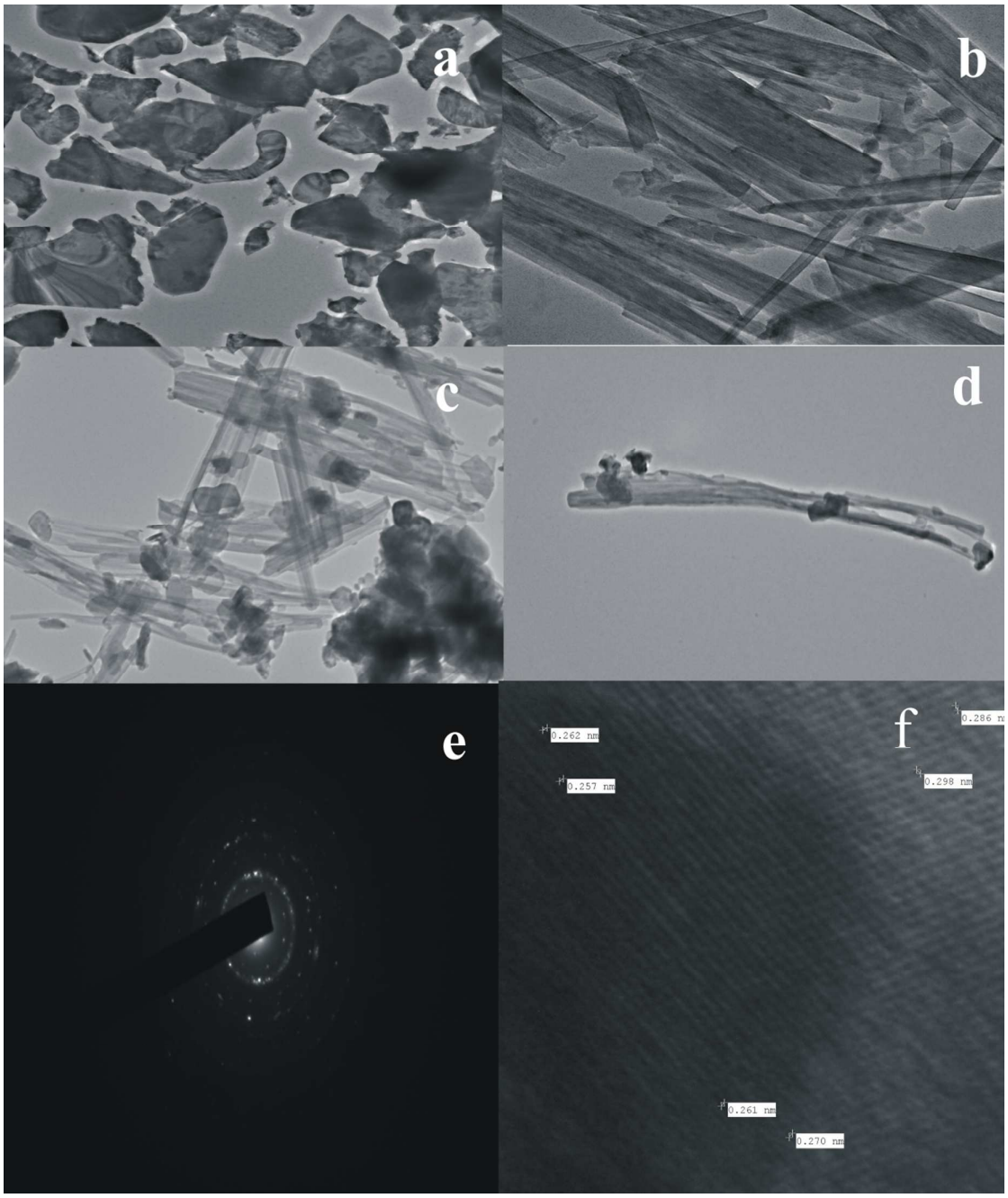

Fig.3. HRTEM images: (a) BiOBr, (b) $Cd(OH)_2$ nanowires, (c-d) BC-50 nanocomposite , (e) SAED pattern of BC-50 and (f) Lattice pattern of the BC-50 composite

The $Cd(OH)_2$ nanowire and BiOBr nanosheet are in proximity, indicating the intimate contact of the two. As depicted in Fig. 3(e), the corresponding SAED pattern displays a spot pattern, indicating the diffused crystalline characteristic of the obtained nanocomposite. The clear

lattice fringe with a spacing of 0.286 and 0.261 nm can be matched well with the tetragonal (110) and hexagonal (101) plane of BiOBr and $Cd(OH)_2$, respectively.[43b,c,d,e]

Interestingly, the intimate contact facilitates the heterojunction construction at the interface, which is beneficial to separate the photogenerated charge carriers, thereby improving the photocatalytic activity.

In Energy Dispersive Spectroscopy (EDS, see ESI), characteristic peaks associated with O, Br, Bi, Cd, and C were observed for BC-50. The Cd and O peaks resulted due to $Cd(OH)_2$ and Bi, Br, O peaks resulted due to BiOBr, respectively, and hence confirmed that the composite was composed of BiOBr and $Cd(OH)_2$. The peak of C atom observed in the spectrum could be attributed to the carbon present on the adhesive tape used to hold the sample.[42]

3.3. Optical Properties

The optical properties of the synthesized BiOBr, $Cd(OH)_2$, and BiOBr/$Cd(OH)_2$ samples were investigated using UV–Vis. Diffuse Reflectance Spectroscopy (UV-DRS) and the results are shown in Fig. 4(c).

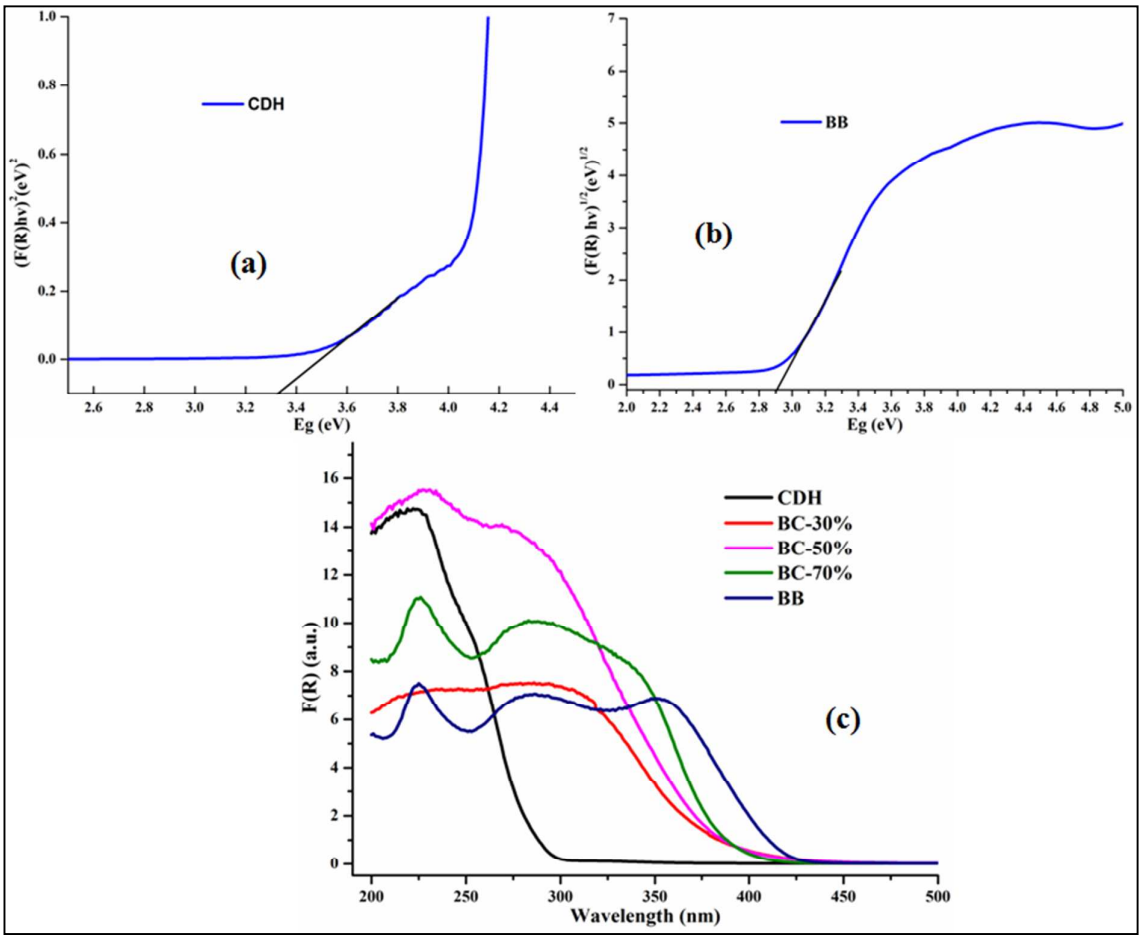

Fig.4. Band gap calculation of (a) $Cd(OH)_2$ and (b) BiOBr, (c) UV-DRS spectra of the various samples.

According to the spectra obtained, the BiOBr sample exhibited strong absorption in the wavelength below 450 nm region of visible light, while the $Cd(OH)_2$ sample exhibited strong absorption in the wavelength range below 300 nm. The BiOBr/$Cd(OH)_2$ composite samples undergo red shift as compared with $Cd(OH)_2$, and this was attributed to BiOBr, being coupled with $Cd(OH)_2$, and hence acting as a sensitizer to extend the optical response.

The decreased band gap and formation of matching trapping sites resulted in good visible light response, appropriate redox centres and hence enhanced photocatalytic performance. These results confirmed that the efficient visible light absorption and photocatalytic activity was caused by the synergistic effect of $Cd(OH)_2$ and BiOBr, and the content of BiOBr was

thought to play a crucial role in the BiOBr/$Cd(OH)_2$ composites. The band gap of the photocatalysts was calculated according to the formula[44]:

$$(h\nu.\alpha) = (Ah\nu - Eg)^{n\backslash 2} \qquad (3)$$

Since α is proportional to Kubelka–Munk function F(R), the expression becomes

$$h\nu.\ F(R) = (Ah\nu - Eg)^{\ n\backslash 2} \qquad (4)$$

ν is the light frequency, F(R) is the Kubelka–Munk function, A is the proportionality constant and Eg is the Band gap energy. The value of n is determined by the type of optical transition (n = 1 for direct transition and n = 4 for indirect transition).[44] The value of n for $Cd(OH)_2$ and BiOBr is 1 and 4 respectively. The Eg of $Cd(OH)_2$ was determined from the plot of $(F(R)\bullet h\nu)^2$ versus $h\nu$ (Fig. 4(a)) and was elicited to be 3.35 eV. Accordingly, the Eg of BiOBr was found to be 2.85 eV from the plot of $(F(R)\ h\nu)^{1/2}$ versus $h\nu$ (Fig. 4(b)).

The valence band edge position of BiOBr/$Cd(OH)_2$ heterostructure at the point of zero charge can be calculated by the following empirical equation[45, 46]:

$$E_{VB} = X - E^c + 0.5E_g \qquad (5)$$

where E_{VB} is the VB edge potential, X is the electronegativity of the semiconductor, and E^c is the energy of free electrons on hydrogen's scale (4.5 eV). Herein, X is the geometric mean of the electronegativity of the constituent atoms. The X values for BiOBr and Cd $(OH)_2$ are ca. 6.18 and 6.65eV, respectively. The top of the valence band E_{VB} of BiOBr and $Cd(OH)_2$ were calculated to be 3.10 eV/NHE and 3.82 eV/NHE respectively. Moreover, conduction band edge potential E_{CB} can be determined by:

$$E_{CB} = E_{VB} - E_g \qquad (6)$$

Thus, the calculated E_{CB} for BiOBr and $Cd(OH)_2$ are 0.25 eV/NHE and 0.47 eV/NHE, respectively.

3.4. Photocatalytic Activity

The photocatalytic performance of the as prepared samples on the decolorization of RhB molecules under visible light irradiation was investigated in mild alkaline conditions, and the results are shown in Fig. 5(a-e).

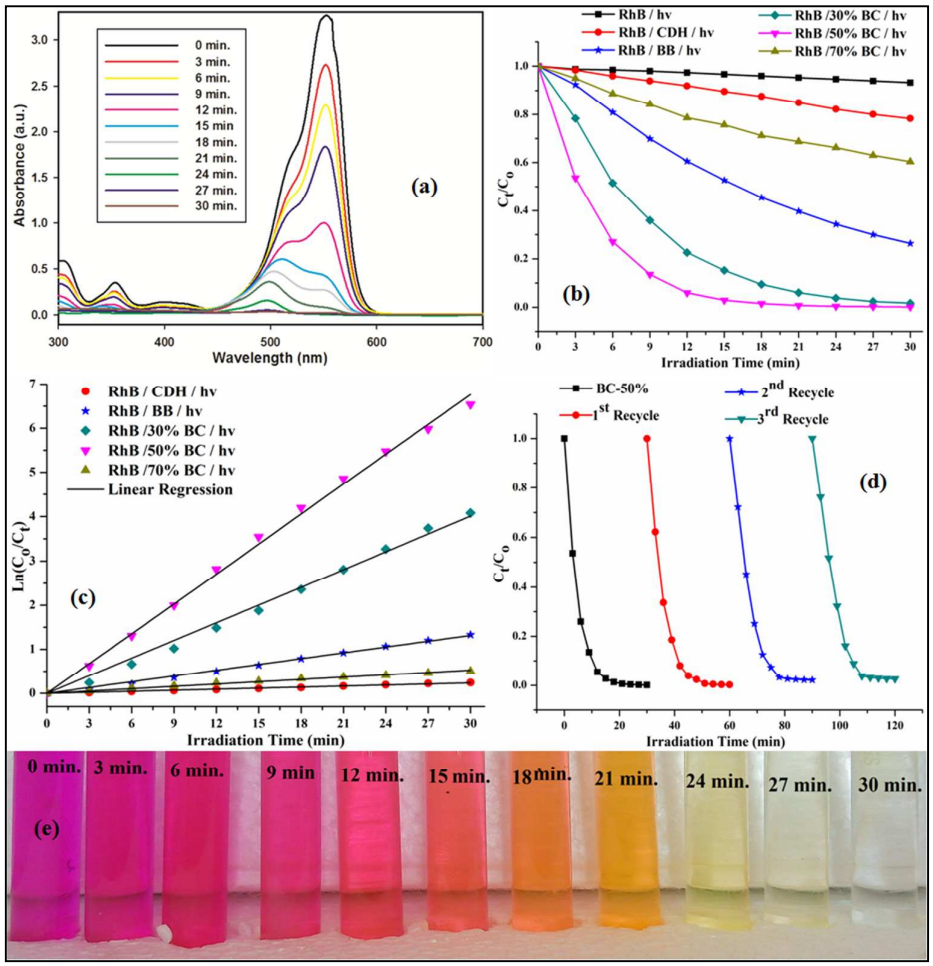

Fig.5. Kinetics of Photocatalytic decolorization of RhB in the presence of pure BB, CDH and and $BiOBr/Cd(OH)_2$ heterostructures. (a) Change in absorption of RhB after regular intervals of light irradiation in presence of BC-50 photocatalyst, (b)Change in concentration (C_t/C_o) of RhB during its decolorization in the presence of CDH, BB and $BiOBr/Cd(OH)_2$ heterostructures, (c) $ln(C_o/C_t)$ versus irradiation time for decolorization of RhB in the presence of different catalysts, (d) Cycling runs of BC-50 for decolorization of RhB under visible light (e) Change in colour of RhB dye at regular intervals of irradiation in the presence of BC-50.

In the control experiments, no decolorization of RhB was observed in the dark, and in the absence of photocatalyst respectively, indicating that RhB was stable and did not undergo a photolytic process. In addition, the catalytic degradation was negligible, suggesting that a purely photocatalytic reaction mechanism took place.

The final decolorization of RhB was only 21.69% by pure $Cd(OH)_2$ under visible light irradiation. The little efficiency was due to the large band gap and agglomeration of $Cd(OH)_2$ nanoparticles, reducing the specific surface areas and the visible light absorption.

The photocatalysis test performed using pure BiOBr resulted in the decolorization of about 73.63% of RhB under visible light in 30 min. As is shown in Fig. 5(b), the 50% BiOBr/$Cd(OH)_2$ (BC-50) composite catalysts exhibited the highest photocatalytic activities. The decolorization of RhB was 99.85%, which was about 4.60 and 1.35 times greater than that of $Cd(OH)_2$ and BiOBr, respectively. The experimental data was found to fit well with the first order kinetic equation. Also from Fig.5(c), the BC-50 composite catalyst was found to exhibit the highest photodegradation efficiency, where the k_{app} of BC-50 was 0.2255 min^{-1}, which was 28.5 and 5.1 times higher than $Cd(OH)_2$ (0.0079 min^{-1}) and BiOBr (0.0439 min^{-1}) respectively. This suggested that BiOBr nanoparticles contributed to the higher redox potentials with well-aligned band-structures and heterostructure interfaces were favourable for the separation of electrons and holes, leading to an enhanced photocatalytic performance. The effect of BiOBr loading amount on the photocatalytic activity was investigated, and the results are shown in Table 1.

Catalyst	% Decolorization	$K_{app}(min^{-1})$
Blank	6.7	0.0023
CDH	21.69	0.0079
BC-70	39.58	0.0176
BB	73.63	0.0439
BC-30	98.31	0.1337
BC-50	99.85	0.2255

TABLE 1: Percentage decolorization and apparent rate constant by different samples

However, the further increase of BiOBr content led to a decrease in RhB decolorization, where the 70% BiOBr/$Cd(OH)_2$ composite exhibited only 50% decolorization.

Although coupling $Cd(OH)_2$ and BiOBr was beneficial for charge separation in the BiOBr/$Cd(OH)_2$ composite, excessive loading of BiOBr particles caused agglomeration and surface coverage of $Cd(OH)_2$, hinder the transfer of charge, and reduced the density of active sites on the $Cd(OH)_2$ surface.[47] The BC-50 composite was thought to cause an effective contact and separation of electrons and holes, resulted in an optimal photocatalytic activity. In order to validate its photocatalytic activity, it was subjected to the photocatalytic degradation of non-dye pollutant, p-chlorophenol (PCP). It was found that BC-50 showed efficient performance for PCP degradation, ruling out the exclusive dye sensitized photocatalysis by the catalyst (Fig.6). The rate constant (K_{app}) for the phenolic degradation was found as 0.068 min^{-1}, 0.044 $min^{-1}$and 0.0025 min^{-1} for BC-50, BB and CDH respectively.

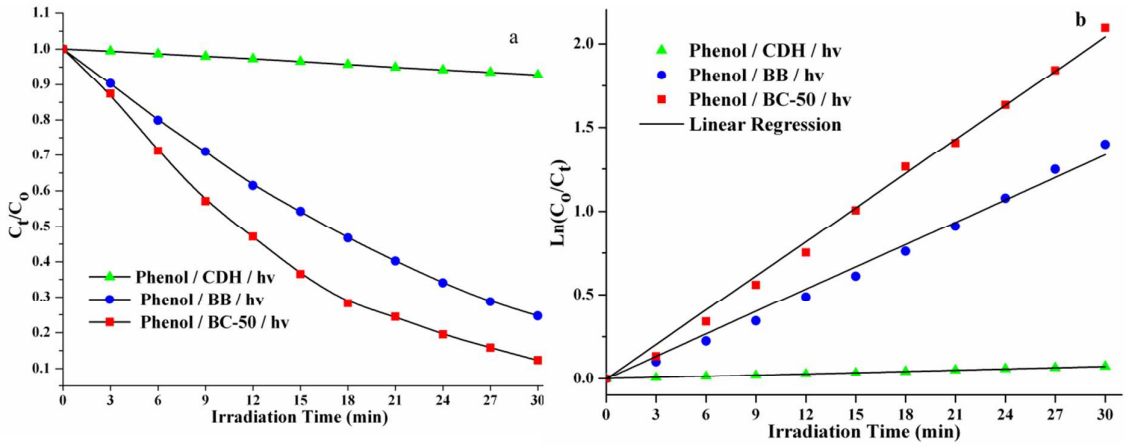

Fig. 6. Kinetics of Photocatalytic degradation of p-chlorophenol in the presence of pure BB, CDH and and BC-50 heterostructures. (a) Change in concentration (C_t/C_o) of PCP during its degradation in the presence of CDH, BB and BC-50 (b) $\ln(C_o/C_t)$ versus irradiation time for degradation of PCP in the presence of different catalysts.

It is worth noting that the $Cd(OH)_2$ and the $BiOBr/Cd(OH)_2$ nanocomposite samples display superior photocatalytic activity in the alkaline pH. These results clearly demonstrate that the photocatalytic activity of the $BiOBr/Cd(OH)_2$ samples can be enhanced under basic conditions.

In view of the practical applications, besides the efficiency, the stability and durability are also indispensable to photocatalysts. To evaluate the stability of the BC-50 composite catalyst, the photocatalytic activity was investigated in cycling runs and the results are shown in Fig. 5(d). In our recycling experiments of RhB photo decolorization in the alkaline pH conditions, the $BiOBr/Cd(OH)_2$ samples exhibited a minimal decrease in activity after four cycles. The stability of the structure and properties ensures that $BiOBr/Cd(OH)_2$ heterostructures can be used as efficient and stable photocatalysts under mild alkaline conditions. In this study, the possible reasons to explain the enhanced photocatalytic properties and structural stability of $BiOBr/Cd(OH)_2$ superstructures in the presence of NaOH is the different solubility behaviour of $Cd(OH)_2$ or $BiOBr/Cd(OH)_2$ in the presence and absence of the base. The K_{sp} of $Cd(OH)_2$ is 5.27 in deionized water. In the presence of base, all $Cd(OH)_2$ or $BiOBr/Cd(OH)_2$ samples possess a much lower solubility, leading to their enhanced stability during the photocatalytic process. Further, it checks the leaching of cadmium ions in the dye solution and hence nullifies its toxic effects as investigated by Atomic Absorption Spectroscopy (Fig. 7). It can be seen that the concentration of Cd ions in the solution phase is lower at alkaline pH than at neutral pH.

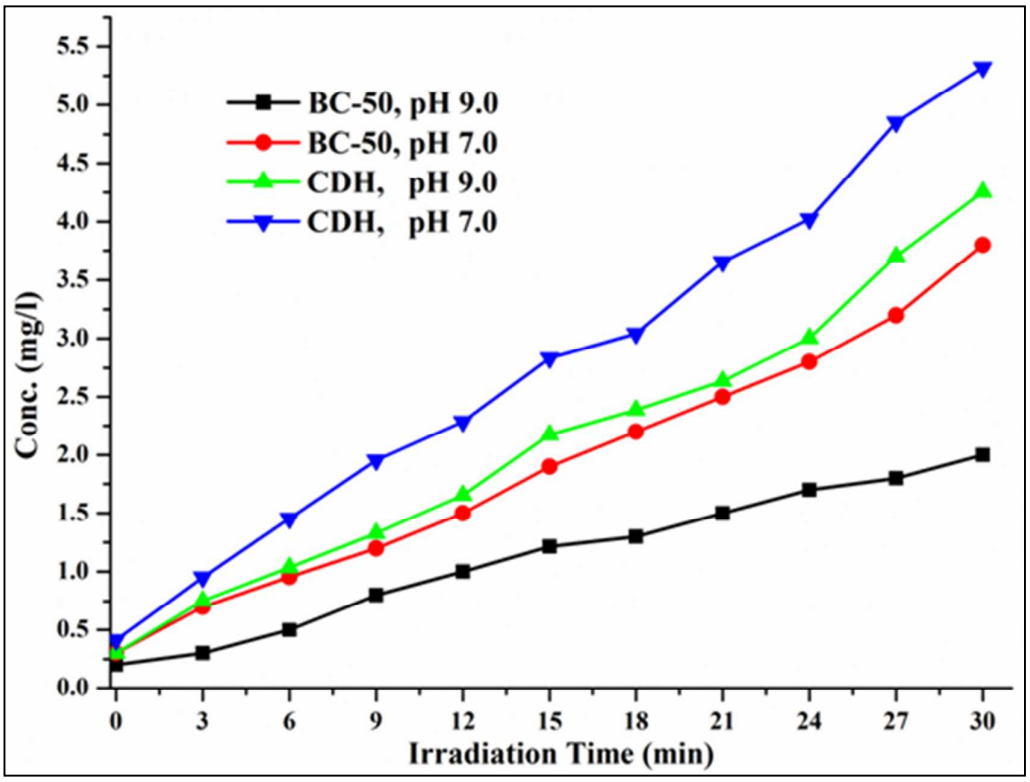

Fig.7. Change in concentration of cadmium ions in dye solutions after regular intervals of irradiation as a result of leaching in the catalysts.

Further, in the photodegradation process, transport of the photogenerated holes is easier in the presence of a base than in the absence of a base. Currently, the photoinduced electron transfer to the CB of $Cd(OH)_2$ results in a charge separation, which hinders the recombination. Thus, the $BiOBr/Cd(OH)_2$ photocatalyzed RhB degradation rate may be significantly accelerated via alkaline conditions.[42]

3.5. Possible Photocatalytic Mechanism

3.5.1. Role of Reactive Species

The radical and hole trapping experiments (scavenger tests) with different scavenger molecules were carried out to elucidate the mechanism of photocatalytic degradation of RhB under visible light irradiation over $BiOBr/Cd(OH)_2$ nanocomposite. Generally, the reactive species such as, hydroxyl radicals ($^{\bullet}OH$), superoxide radical anions ($O_2^{-\bullet}$) and holes (h^+) are expected to be involved in the photocatalytic dye decolorization processes.

The roles of the reactive species were investigated through radical and hole trapping experiments and the results obtained are shown in Fig. 8.

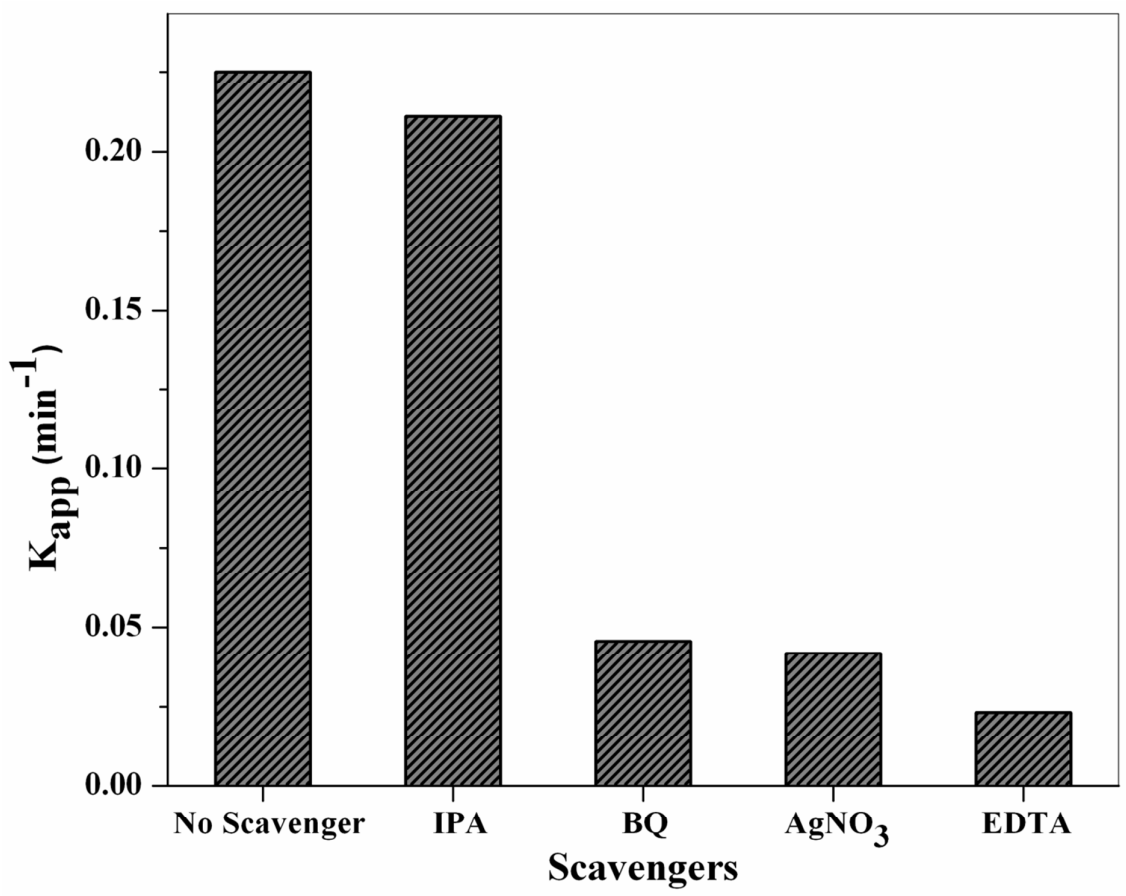

Fig.8. Effect of various scavengers on the photocatalytic activity of BC-50 for thedecolorization of RhB.

The decolorization of RhB decreased slightly upon the addition of isopropyl alcohol (IPA, a hydroxyl radicals scavenger[48]), indicating that dissolved •OH radicals were not the dominant active species in this process. In contrast, the addition of disodium ethylenediaminetetraacetate (EDTA, a hole scavenger[49]) had a significantly negative effect on the degradation of RhB, confirming that the holes were the dominant active species. Upon addition of benzoquinone (BQ) [50a], a scavenger to quench $O_2^{-\bullet}$, the k_{app} dropped remarkably, indicating that $O_2^{-\bullet}$radicals were another active species in the reactive system. The electron

scavenger[50b,c], $AgNO_3$, addition decreased the rate considerably, hence indicating electron mediated degradation mechanism. The substantial electron dependence depict that the electron transfer along the composite catalysts has role in superoxide radical formation.

The above results demonstrated that the photocatalytic process was mainly governed by direct holes and $O_2^{-\bullet}$ oxidation reactions while free hydroxyl radicals were negligible.

3.5.2. Band gap structures and possible degradation mechanism

Photocatalytic performance of a composite photocatalyst depends on its heterojunction interface, and the electronic structures[51], because the photocatalytic activity is closely related to the conduction band (CB) and the valence band (VB), as well as to the mobility of the carriers. CB and VB could determine the oxidative and reductive ability of the catalyst, respectively, while the mobility of the charge carriers could determine the photocatalytic efficiency. For metal oxide photocatalysts, the VB consists of the 2p orbital of oxygen, but for bismuth-based semiconductors, the VB is a hybrid of the 2p orbital of oxygen and 6s orbital of Bi, and the CB is composed of the 6p orbital of Bi[25, 52], which possesses a highly reductive capability.

The light energy utilization ratio and the effective separation of photogenerated charge carriers are favourable for photocatalytic activity.[27] The BiOBr/$Cd(OH)_2$ composites exhibited a good light energy utilization ratio, which could photoexcite the charge carriers. It was reported that the well-matched overlapping band-structure in the composite could promote the separation of electron and holes, thereby improving the photocatalytic activity.[53]

The band edge positions of BiOBr and $Cd(OH)_2$ were estimated according to the methods discussed above.[28] These results confirmed that BiOBr and $Cd(OH)_2$ possessed a good composite structure, which was favourable for the separation of the photogenerated carriers. On the basis of band gap structure of as-prepared BiOBr/$Cd(OH)_2$ and the effects of

scavengers, possible pathways for the photocatalytic decolorization were proposed as follows.

In these samples, BiOBr is a p-type semiconductor, whereas $Cd(OH)_2$ is an n-type semiconductor. The formation of the p–n junction could lead to an efficient electron–hole separation that minimized the recombination of photoexcited electron–hole pairs.[54] The valence bands (VB) and conduction bands (CB) of BiOBr (E_{VB}= 3.10 eV, E_{CB}= 0.25 eV); and $Cd(OH)_2$ (E_{VB}= 3.82 eV, E_{CB}= 0.47 eV) were provided to clearly clarify the separation and transfer of electron–hole pairs at the interface of the heterostructures. The Fermi level (E_F) of n-type Cd $(OH)_2$ was close to the conduction band, whereas the E_F of p-type BiOBr was close to the valence band. When p-type BiOBr and n-type $Cd(OH)_2$ formed p–n junctions, the E_F of $Cd(OH)_2$ and BiOBr were aligned, and when the E_F reached equilibration, the internal electric field with the direction from n-type $Cd(OH)_2$ to p-type BiOBr was built. As a result, the energy bands of $Cd(OH)_2$ shifted downward along with the E_F, whereas those of BiOBr shifted upward and the newly formed energy band structure was obtained[55], as depicted in Fig. 9(b).

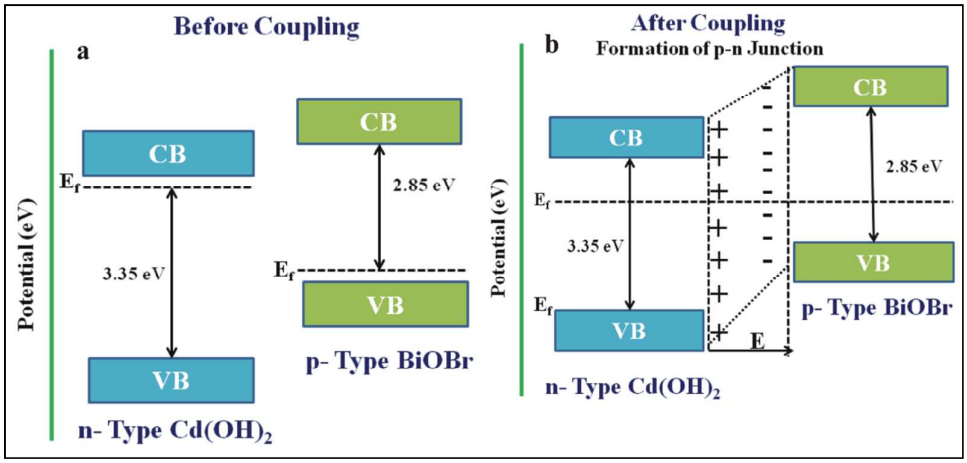

Fig.9. (a) Band gap alignment of $Cd(OH)_2$ and BiOBr nanoparticles before coupling (b) Formation of p-n junction and subsequent energy level alignment on heterostructure formation.

The electrons in the CB of BiOBr would quickly be injected to that of $Cd(OH)_2$. In such a way, the photogenerated electron–hole pairs would be separated effectively by the p–n junction formed in the BiOBr/$Cd(OH)_2$. Contrarily, the CB and VB positions of the single BiOBr and $Cd(OH)_2$ were unfavourable for the separation of electron–hole pairs before contact.

When the BiOBr/$Cd(OH)_2$ composite was irradiated by visible light, only BiOBr could be excited, and the photogenerated electrons and holes could be produced in its CB and VB, respectively. Due to the matching energy band structures and the closely contacted interface and driving force from the internal electric field, the excited electrons produced by BiOBr were injected into the CB of $Cd(OH)_2$. Since the CBM of BiOBr is more negative than that of $Cd(OH)_2$, the CB of $Cd(OH)_2$ would accept these excited electrons from the CB of BiOBr. Meanwhile, the photogenerated holes were effectively accumulated in the VB of BiOBr, as depicted in Fig. 10.

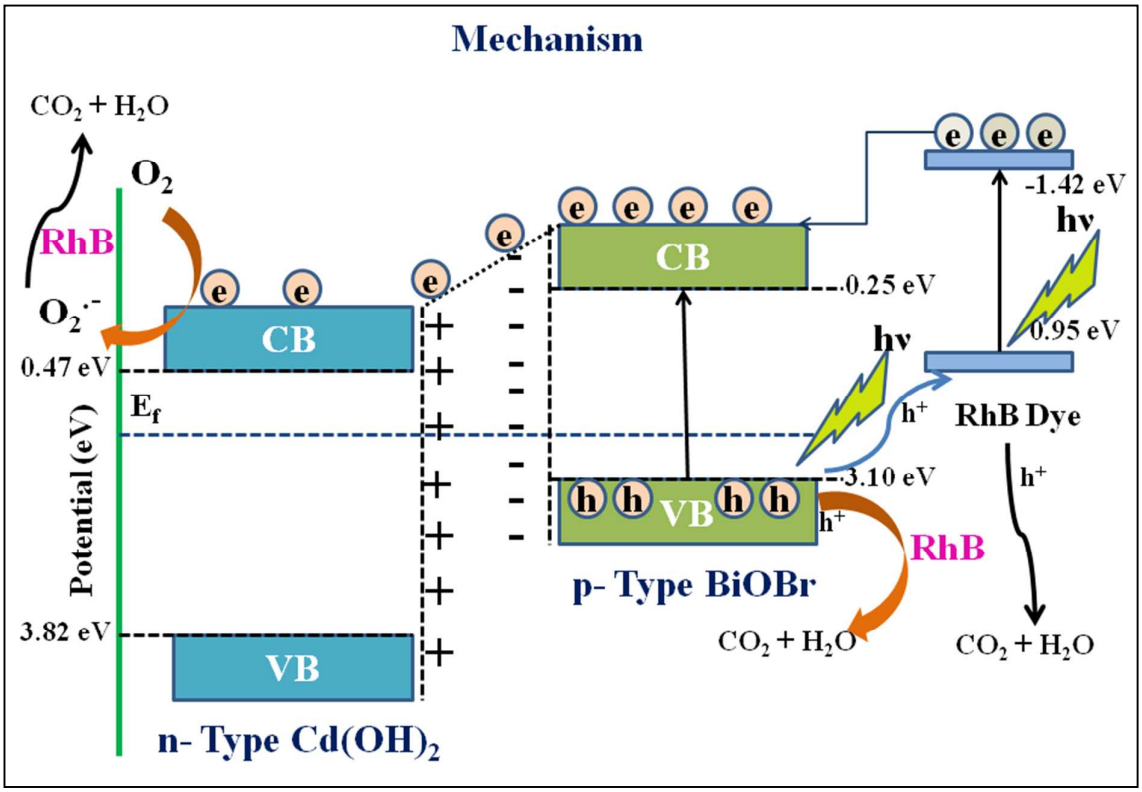

Fig.10. Schematic mechanism and formation of ROS in the photodegradation process by the heterostructure.

This process promoted the efficient charge separation and inhibited the recombination of electrons and holes.

In order to further investigate the transfer of the photogenerated electron–hole pairs between the two semiconductors, the composite were investigated by photoluminescence spectra (PL) and were presented in Fig. 11, for pure BiOBr and the BiOBr/$Cd(OH)_2$ composite (using an excitation wavelength of 280 nm). A main emission peak was observed at about 445 nm for the pure BiOBr, which was attributed to recombination of electron–hole pairs in the BiOBr material.[43] The intensity of this emission peak gradually decreased upon BiOBr loading upto 50% BiOBr/$Cd(OH)_2$ ratio, without changing the fluorescence emission peak position. This indicated that the recombination of the photo-excited electrons and holes was greatly reduced by coupling the BiOBr and $Cd(OH)_2$.

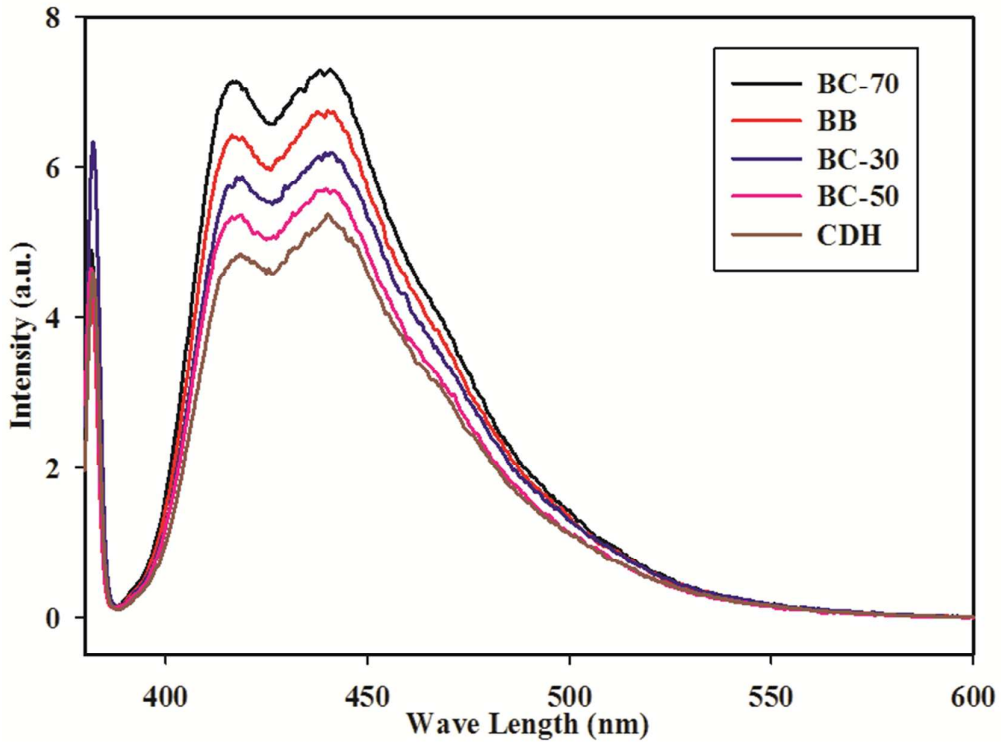

Fig.11. Photoluminescence (PL) spectra of various photocatalyst samples

The lower PL peak intensity in BC-50 sample than the other suggested the highest separation and transfer efficiency of photogenerated electron–hole pairs and resulted in its improved photocatalytic activity. As can be seen, $Cd(OH)_2$ exhibited lowest PL intensity due to its large band gap and subsequent small response and separation of the charge carriers on excitation.

Based on the potential of conduction band edge, it can be inferred that the composite is unable to reduce the dissolved oxygen on $Cd(OH)_2$ surface, that requires −0.28 eV/NHE for the formation of superoxide anion radicals. However, the addition of base facilitated the superoxide formation by influencing the redox potential of $O_2/O_2^{-\bullet}$. The photogenerated electrons in the CB of the $Cd(OH)_2$ could thus be captured by adsorbed O_2 to generate reactive $O_2^{-\bullet}$ radicals.[42,56] Furthermore, the VB edge standard redox potentials of BiV/BiIII[57] were less positive than E^0 ($^{\bullet}OH/OH^-$) (+2.38 eV)[58], confirming that the photogenerated holes could not oxidize OH^- to yield $^{\bullet}OH$. The enriched OH radical were very active, and could decompose RhB directly[27]. As the formed hydroxyl radicals are quite scarce, it indicated that the photogenerated holes would play a dominant role in the photocatalytic system of BiOBr/$Cd(OH)_2$ heterojunctions.

Under photocatalytic conditions, three possible mechanisms might explain the degradation of the dye on the surface of the semiconductor. In addition to the semiconductor photocatalytic mechanism, the dye-sensitized mechanism and dye-photolysis mechanism may also exist.[59]

The potential of HOMO−LUMO levels of RhB (E_{HOMO} = 0.95 eV and E_{LUMO} = −1.42 eV that matches fairly well with the λ_{max} of 553 nm).[60, 61] It is clear from Fig. 10 that, although the excited electrons of RhB can inject into the CB of BiOBr, they are ineffective to further react with absorbed O_2, as they readily move down to the CB of $Cd(OH)_2$.[27]

Moreover, the positioning of E_{VB} below the HOMO levels of RhB is suitable for hole transfer from BiOBr to adsorbed dye molecules and supportive for the role of holes in RhB degradation.[34]

Based on the above assumption, a plausible photocatalytic process was proposed, as illustrated in Fig. 10. Firstly, the dye molecules are easily adsorbed on the catalyst surface. The adsorbed RhB can be excited by visible light irradiation and inject electrons into the conduction band of the catalyst to form $O_2^{-\bullet}$. Simultaneously, the photo-induced holes are capable of oxidizing RhB directly[62] and the photo-generated electrons was also believed to enhance the oxidation process through reduction of absorbed O_2 into $O_2^{-\bullet}$.[63] Finally, the $O_2^{-\bullet}$and h_{VB}^{+} can oxidize the RhB molecules to CO_2 and H_2O.

In general, these dyes are subjected to de-ethylation accompanied by a ring-opening reaction of the benzene rings during the photocatalytic degradation.[64, 65] Rhodamine B (λ_{max} 554 nm) could convert to Rhodamine (λ_{max} 498 nm) via de-ethylation in the photocatalytic process. In the de-ethyl RhB, the benzene rings are constantly attacked by positive holes till complete degradation of the molecule. The blue-shift of the maximum absorption peak Fig. 5(a) could correspond to the de-ethylation of RhB. With the de-ethylation step, the absorption peak was gradually blue-shifted from 554 to 552 nm, then to 510 nm, and finally to 498 nm, which was apparently observed with the gradual change of colour from pink to yellow, Fig. 5(e).[25]

4. Conclusions

In summary, BiOBr/$Cd(OH)_2$ composite photocatalysts were synthesized by a simple precipitation method. The composites prepared exhibited strong visible light absorption and red shift in the visible light region. The 50% BiOBr loaded cadmium hydroxide could degrade about 99.85% of Rhodamine B dye under irradiation for 30 min, where the photocatalytic activity did not show significant decrease after four cycles of reuse. It was also found that holes enriched in the valence band of BiOBr and the $O_2^{-\bullet}$ radicals formed at conduction band of $Cd(OH)_2$ played a dominant role in the oxidation of Rhodamine B in the BiOBr/$Cd(OH)_2$ system. The high photocatalytic activity could be attributed to the enhanced

light absorption and the improved separation of photogenerated charge carriers, due to the closely contacted interface and the matched energy level structure in the prepared materials.

It was also concluded that the photocatalytic efficiency increased drastically under mild alkaline pH due to the stability of the catalyst to dissolution and improved charge mobility.

Acknowledgements

BM Pirzada thanks CSIR New Delhi for Junior Research Fellowship. NA Mir thanks DST for Young Scientist grant. The authors are also thankful to DST and UGC, India for research support in the form of FIST/PURSE and DRS II grants to the Department of Chemistry, Aligarh Muslim University, India. Contributions from Department of Physics, Aligarh Muslim University for PXRD and UV-DRS facilities; and USIF, Aligarh Muslim University for SEM, TEM and EDS studies are gratefully acknowledged.

References

[1] Y.J. Wang, X.J. Bai, C.S. Pan, J. He, Y.F. Zhu, J. Mater. Chem., 2012, 22, 11568.

[2] H. Xie, Y. Li, S. Jin, J. Han, X. Zhao, J. Phys. Chem. C, 2010, 114, 9706.

[3] M. Tabata, K. Maeda, T. Ishihara, T. Minegishi, T. Takata, K. Domen, J. Phys. Chem. C, 2010, 114, 11215.

[4] H.S. Jung, Y.J. Hong, Y. Li, J. Cho, Y.J. Kim, G.C. Yi, ACS Nano, 2008, 2, 637.

[5] J.H. Huang, Y.J. Cui, X.C. Wang, Environ. Sci. Technol., 2010, 44, 3500.

[6] Z.G. Zou, J.H. Ye, K. Sayama, H. Arakawa, Nature, 2001, 414, 625.

[7] X.Z. Bu, G.K. Zhang, C.H. Zhang, Applied Surface Science, 2012, 258, 7997.

[8] Y.J. Lin, S. Zhou, X.H. Liu, S. Sheehan, D.W. Wang, J. Am. Chem. Soc., 2009, 1312772.

[9] I. Nakamura, N. Negishi, S. Kutsuna, T. Ihara, S. Sugihara, K. Takeuchi, J. Mol.Catal. A: Chem., 2000, 161, 205.

[10] B. Jiang, S. Zhang, X. Guo, B. Jin, Y. Tian, Appl. Surf. Sci., 2009, 255, 5975.

[11] R. Zheng, X. Meng, F. Tang, Appl. Surf. Sci., 2009, 255, 5989.

[12] (a) W. Zhao, W. Ma, C. Chen, J. Zhao, Z. Shuai, J. Am. Chem. Soc., 2004, 126, 4782. (b) M-Q Yang, N. Zhang, M. Pagliaro,Y-J Xu, Chem. Soc. Rev., 2014, 43, 8240. (c) N. Zhang, Y. Zhang,Y-J Xu, Nanoscale, 2012, 4, 5792. (d) C. Han, M-Q Yang, B. Weng,Y-J Xu, Phys.Chem.Chem.Phys., 2014, 16, 16891. (e) X. Pan, M-Q Yang, X. Fu, N. Zhang,Y-J Xu, Nanoscale, 2013, 5, 3601.

[13] X.B. Chen, S.H. Shen, L.J. Guo, S.S. Mao, Chem. Rev., 2010, 110, 6503.

[14] P.V. Kamat, J. Phys. Chem. C, 2007, 111, 2834.

[15] X. Wei, T.F. Xie, D. Xu, Q.D. Zhao, S. Pang, D.J.Wang, Nanotechnology, 2008, 19, 275707.

[16] X. Wei, T.F. Xie, L.L. Peng, W. Fu, J.S. Chen, Q. Gao, G.Y. Hong, D.J. Wang, J. Phys. Chem. C, 2011, 115, 8637.

[17] J. Jiang, X. Zhang, P.B. Sun, L. Zhang, J. Phys. Chem. C, 2011, 115, 20555.

[18] M. Shang, W. Wang, L. Zhang, J. Hazard. Mater., 2009, 167, 803.

[19] H. Cheng, B. Huang, P. Wang, Z. Wang, Z. Lou, J. Wang, X. Qin, X. Zhang, Y. Dai, Chem. Commun., 2011, 47, 7054.

[20] J. Henle, P. Simon, A. Frenzel, S. Scholz, S. Kaskel, Chem. Mater., 2007, 19, 366.

[21] Z. Jiang, F. Yang, G.D. Yang, L. Kong, M.O. Jones, T.C. Xiao, P.P. Edwards, J. Photochem. Photobiol. A, 2010, 212, 8.

[22] G.H. Jiang, X.H. Wang, Z. Wei, X. Li, X.G. Xi, R.B. Hu, B.L. Tang, R.J. Wang, S. Wang, T. Wang, W.X. Chen, J. Mater. Chem. A, 2013, 1, 2406.

[23] J. Zhang, F.J. Shi, J. Lin, D.F. Chen, J.M. Gao, Z.X. Huang, X.X. Ding, C.C. Tang, Chem. Mater., 2008, 20, 2937.

[24] W. Wang, F. Huang, X. Lin and J. Yang, Catal. Commun., 2008, 9, 8.

[25] F. Shen, L. Zhou, J.J. Shi, M.G. Xing, J.L. Zhang, RSC Adv., 2015, 5, 4918.

[26] G.H. Jiang, R.J. Wang, X.H. Wang, X.G. Xi, R.B. Hu, Y. Zhou, S. Wang, T. Wang, W.X. Chen, ACS Appl. Mater. Interfaces, 2012, 4, 4440.

[27] J. Fu, Y.L. Tian, B.B. Chang, F.N. Xia, X.P. Dong, J. Mater. Chem., 2012, 22, 21159.

[28] L. Kong, Z. Jiang, H.H. Lai, R.J. Nicholls, T.C. Xiao, M.O. Jones, P.P. Edwards, J. Catal., 2012, 293, 116.

[29] Y.L. Li, Y.M. Liu, J.S. Wang, E. Uchaker, Q.F. Zhang, S.B. Sun, Y.X. Huang, J.Y.Li, G.Z. Cao, J. Mater. Chem. A, 2013, 17949.

[30] R.S. Mane, S.-H. Han, Electrochem. Commun., 2005, 7, 205.

[31] A. Kudo, K. Omori, H.J. Kato, J. Am. Chem. Soc., 1999, 121, 11459.

[32] J. Tang, Z. Zou, J. Ye, Angew. Chem., Int. Ed., 2004, 43, 4463.

[33] H. G. Kim, D. W. Hwang, J. S. Lee, J. Am. Chem. Soc., 2004, 126, 8912.

[34] G.P. Naresh, T. K. Mandal, ACS Appl. Mater. Interfaces, 2014, 6, 21000.

[35] N.A. Mir, M.M. Haque, A. Khan, K. Umar, M. Muneer, S. Vijayalakshmi, J. Adv. Oxid. Technol., 2012, 15, 380.

[36] N.Z. Bao, L.M. Shen, T.S. Takata, K. Domen, Chem. Mater., 2008, 20, 110.

[37] N. Guettaï, H. A. Amar, Desalination, 2005, 185, 427.

[38] C.-H. Wu, H.-W. Chang, J.-M. Chern, J. Hazard. Mater., 2006, 137, 336.

[39] G.T. Li, K.H. Wong, X.W. Zhang, C. Hu, J.C. Yu, R.C.Y. Chan, P.K. Wong, Chemosphere, 2009, 76, 1185.

[40] N. Zhang, S.Q. Liu, X.Z. Fu, Y.J. Xu, J. Phys. Chem. C, 2011, 115, 9136.

[41] J. Cao, B. Xu, H. Lin, B. Luo, S. Chen, Chem. Eng. J., 2012, 185–186, 91.

[42] Z. -Q. Li, X. –S. Lin, L. Zhang, X. –T. Chen, Z. –L. Xue, Cryst Eng Comm, 2012, 14, 3495.

[43] (a) W.Q. Cui, W. An, L. Liu, J.S. Hu, Y.H. Liang, App. Surf. Sci., 2014, 319, 298. (b) H.P. Jiao, X. Yu, Z.Q. Liu, P.Y. Kuang, Y.M. Zhang, RSC Adv., 2015,5, 16239. (c) D.Q. Zhang, M.C. Wen, B. Jiang, G. Li, J.C. Yu, J. Hazard. Mater., 2012, 211– 212, 104. (d) M.F.

Ye, H.Z. Zhong, W. Zheng, R. Li,Y.F. Li, Langmuir, 2007, 23, 9064. (e) V. Eskizeybek, O. Demir, A. Avci, M. Chhowalla, J Nanopart Res, 2011, 13, 4673.

[44] M.A. Butler, J. Appl. Phys., 1977, 48, 1914.

[45] O. Mehraj, N.A. Mir, B.M. Pirzada, S. Sabir, M. Muneer, J. Mol. Catal. A: Chem., 2014, 395, 16.

[46] X. Zhang, L. Zhang, T. Xie, D. Wang, J. Phys. Chem. C, 2009, 113, 7371.

[47] J. Xia, J. Di, S. Yin, H. Xu, J. Zhang, Y. Xu, L. Xu, H. Li, M. Ji, Adv., 2014, 4, 82.

[48] C. Hu, T.W. Peng, X.X. Hu, Y.L. Nie, X.F. Zhou, J.H. Qu, H. He, J. Am. Chem. Soc., 2010, 132, 857.

[49] M.C. Yin, Z.S. Li, J.H. Kou, Z.G. Zou, Environ. Sci. Technol., 2009, 43, 8361.

[50] (a) W.Q. Cui, Y.F. Liu, L. Liu, J.S. Hu, Y.H. Liang, Appl. Catal. A: Gen., 2012, 417, 111. (b) N. Zhang, M-Q Yang, Z-Rg Tang, Y-J Xu. ACS NANO, 2014, 8, 623. (c) Z. Chen, N. Zhang,Y-J Xu, CrystEngComm, 2013, 15, 3022.

[51] M. Sathish, B. Viswanathan, R. P. Viswanath, C. S. Gopinath, Chem. Mater., 2005, 17, 6349.

[52] J. Tang, Z. Zou and J. Ye, Angew. Chem., Int. Ed., 2004, 43, 4463.

[53] C.L. Yu, G. Li, S. Kumar, K. Yang, R.C. Jin, Adv. Mater., 2014, 26, 892.

[54] F.X. Ye, A. Ohmori, C.J. Li, Surf. Coat. Technol., 2004, 184233.

[55] G.P. Dai, J.G. Yu, G. Liu, J. Phys. Chem. C., 2011, 115, 7339.

[56] A. Hameed, M.D. Aslam, I.M.I. Ismail, N. Salah, P. Fornasiero, Applied Catalysis B: Environmental, 2015, 163, 444.

[57] H.B. Fu, C.S. Pan, W.Q. Yao, Y.F. Zhu, J. Phys. Chem. B, 2005, 109, 22432.

[58] H.F. Cheng, B.B. Huang, Y. Dai, X.Y. Qin, X.Y. Zhang, Langmuir, 2010, 26, 6618.

[59] H. Gerischer, F. Willig, Top. Curr. Chem., 1976, 61, 31.

[60] S. Kumar, T. Surendar, A. Baruah, V. Shanker, J. Mater. Chem. A, 2013, 1, 5333.

[61] L. Pan, J. Zou, X. Liu, X. Liu, S. Wang, X. Zhang, L. Wang, Ind. Eng. Chem. Res., 2012, 51, 12782.

[62] Y. Cao, X.T. Zhang, W.S. Yang, H. Du, Y.B. Bai, T.J. Li, J.N. Yao, Chem. Mater., 2000,12, 3445.

[63] A.L. Linsebigler, G.Q. Lu, J.T. Yates, Chem. Rev., 1995, 95, 735.

[64] T. Wu, G. Liu, J. Zhao, H. Hidaka, N. Serpone, J. Phys. Chem. B, 1998, 102, 5845.

[65] J. Zhuang, W. Dai, Q. Tian, Z. Li, L. Xie, J. Wang, P. Liu, X. Shi, D. Wang, Langmuir, 2010, 26, 9686.

Graphical abstract

- The $BiOBr/Cd(OH)_2$ heterojuction formation decreased the charge recombination phenomenally and imparted significant visible light response.